

9. TURBIDITE FACIES AND BED-THICKNESS CHARACTERISTICS INFERRED FROM MICRORESISTIVITY (FMS) IMAGES OF LOWER TO UPPER PLIOCENE RIFT-BASIN DEPOSITS, WOODLARK BASIN, OFFSHORE PAPUA NEW GUINEA¹

Sherif A.M. Awadallah,² Richard N. Hiscott,² Michael Bidgood,² and Timothy E. Crowther²

ABSTRACT

From the early to late Pliocene, a northward-thinning turbidite succession accumulated on rifted crust of the western Woodlark Basin offshore Papua New Guinea. The source of detritus was to the north and west, resulting in oblique to longitudinal supply into the propagating rift. Formation MicroScanner (FMS) microresistivity images collected in three boreholes along a north-south transect (Holes 1118A, 1109D, and 1115C) were used to construct bed-by-bed sedimentary sections through the turbidite succession, which consists of variable proportions of mud and graded sand and silt turbidites. In all holes, the number of sand and silt turbidite beds decreases exponentially with increasing bed thickness, and there is a significant "tail" of relatively thick beds. Plots in log-log space of the number of beds thicker than T , vs. T , consist of one or two straight-line segments, except for deviations at low values of T near the FMS tool resolution limit. Each straight-line segment suggests a power-law relationship of the form $Y = nT^{-e}$, with e in the range of 1.5–5.5. It is proposed that the underlying control on this pattern is the widely observed power-law distribution of earthquakes.

¹Awadallah, S.A.M., Hiscott, R.N., Bidgood, M., and Crowther, T.E., 2001. Turbidite facies and bed-thickness characteristics inferred from microresistivity (FMS) images of lower to upper Pliocene rift-basin deposits, Woodlark Basin, offshore Papua New Guinea. *In* Huchon, P., Taylor, B., and Klaus, A. (Eds.), *Proc. ODP, Sci. Results*, 180, 1–30 [Online]. Available from World Wide Web: <http://www-odp.tamu.edu/publications/180_SR/VOLUME/CHAPTERS/166.PDF>. [Cited YYYY-MM-DD]

²Earth Sciences Department, Memorial University of Newfoundland, St. John's NF A1B 3X5, Canada. Correspondence author: rhiscott@sparky2.esd.mun.ca

At times, the rate of addition of new sand and silt turbidites to Sites 1118 and 1109 was $\sim 1000\text{--}1500$ beds/ 10^6 yr, whereas Site 1115 never received more than ~ 450 beds/ 10^6 yr. Site 1118, nearest the axis of the rift basin, had the longest history of high-frequency turbidite deposition (~ 1500 beds/ 10^6 yr, equivalent to a recurrence interval of 670 yr). Turbidite recurrence intervals are approximately one order of magnitude longer than the recurrence intervals of ≥ 7 -magnitude earthquakes in this region, suggesting that factors other than the availability of seismic triggers are required to generate turbidity currents. The lower frequency of deposition of sand and silt turbidites north of the axis of the rift, when compared to the turbidite frequency at axial Site 1118, is ascribed to a combination of lateral and distal fining, so that many flows responsible for graded beds of sand and silt at Site 1118 only deposited mud at Sites 1109 and 1115. This mud was subsequently disturbed by burrowing in areas of slow accumulation.

INTRODUCTION

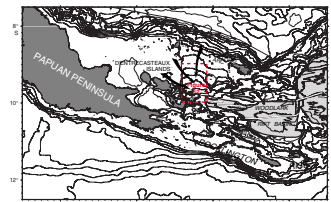
The western Woodlark Basin is a propagating Neogene rift extending eastward from Papua New Guinea and the D'Entrecasteaux Islands (Fig. F1). In the segment of the rift north of the Pocklington Rise and Moresby Seamount, the basin consists of an asymmetric graben atop a north-dipping detachment fault (Taylor et al., 1999; Taylor, Huchon, Klaus, et al., 1999). Sites 1118, 1109, and 1115 were drilled along a transect that extends northward from the basin axis (Fig. F2). Present water depth (~ 2300 m) and thickness of the basin-fill deposits (~ 850 m) are greatest at Site 1118.

The floor of the rift basin experienced a phase of rapid subsidence beginning at ~ 3.9 Ma (late early Pliocene) (Takahashi et al., this volume). Until ~ 3 Ma in the middle Pliocene, accumulation rates ranged from ~ 480 m/m.y. at Site 1118 to ~ 300 m/m.y. at Sites 1109 and 1115 (the Pliocene is divided into three epochs following Shipboard Scientific Party, 1999). Water depth reflected this strong subsidence by increasing rapidly from <150 m before ~ 3.9 Ma (outer neritic) to $500\text{--}2000$ m by ~ 2.5 Ma (middle bathyal). During the phase of rapid subsidence and deepening, rift-basin facies consisted of marine shales punctuated by thin- to thick-bedded sandy and silty turbidites derived from the Papuan Peninsula, D'Entrecasteaux Islands, and Trobriand arc (Robertson et al., in press).

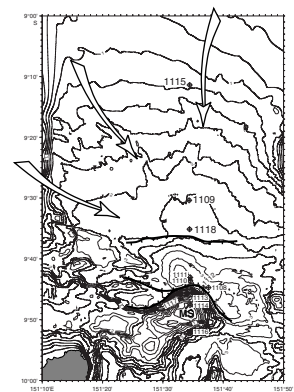
Sandy and silty turbidites interbedded with shales are particularly amenable to study using high-resolution microresistivity logs like the Schlumberger Formation MicroScanner (FMS) tool and its successor, the Formation MicroImager. This is because of the sharp contrast in resistivity between the coarser basal divisions of turbidites and the associated shales. For example, Hiscott et al. (1992, 1993) and Pirmez et al. (1997) used FMS images to document facies architecture and bed-thickness distributions in turbidites from the Izu-Bonin forearc and the Amazon submarine fan, respectively. In the case of these earlier studies, the microresistivity images permitted intervals of low core recovery in Ocean Drilling Program (ODP) boreholes to be described bed by bed just like the intervals that were successfully cored and described at sea.

The lower to upper Pliocene succession in the western Woodlark Basin consists of rhythmically interbedded muds, silt turbidites, and sand turbidites. This interbedding can be appreciated from standard down-hole logs as well as from FMS images. Gamma ray profiles are not suit-

F1. Regional setting of the Woodlark Basin, p. 13.



F2. Location of ODP sites around and north of the Moresby Seamount, p. 14.



able as a guide to textural variations because of radioactive sands in the Woodlark Basin succession. Instead, the difference between neutron porosity (APLC) and lithodensity tool porosity (DPHI), designated as DPORO, serves as a more reliable indicator of clay content and texture (Shipboard Scientific Party, 1999; C  lerier et al., this volume). DPORO varies from -1.8 in uniformly sized sand to 0.4 in clay; poorly sorted sands and silts have intermediate values. Downhole plots of DPORO show a serrated signature at all drill sites because of the fine-scale interbedding of sand and silt turbidites with basinal muds (Fig. F3).

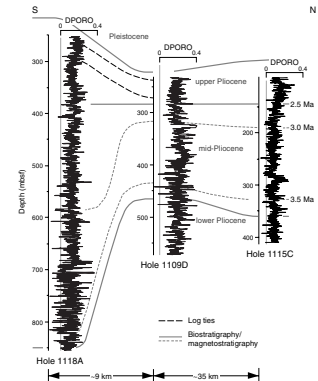
Continuous FMS images in turbidite successions allow the assembly of large data sets that can be used to investigate the nature and origin of particular types of bed-thickness populations like those conforming to exponential or power-law distributions (e.g., Drummond and Wilkinson, 1996; Beattie and Dade, 1996; Malinverno, 1997). Even in the western Woodlark Basin, where core recovery was generally high (commonly $>80\%$), borehole images provide a powerful complement to cores because (1) there are no gaps in the data, and (2) sand bed thicknesses can be determined even in intervals where rotary coring (including extended core barrel coring) has produced drilling "biscuits" (Shipboard Scientific Party, 1995) and core disturbance that prevent accurate determination of bed thicknesses and sedimentary structures.

FMS images from the uppermost lower Pliocene to lowermost upper Pliocene turbidite successions at Sites 1118, 1109, and 1115 were studied with a number of goals in mind: (1) to prepare uninterrupted bed-by-bed sections for studies of sediment architecture, (2) to assess the nature of bed-thickness populations, (3) to investigate turbidity-current frequency as a function of basin tectonics and accumulation rates, and (4) to assess temporal and spatial variability in turbidite facies in a rift setting. The oldest deposits considered at each site date from the time when water depth increased to >150 m (from Takahashi et al., this volume), corresponding to 850 meters below seafloor (mbsf) in Hole 1118A (~ 3.6 Ma), 570 mbsf in Hole 1109D (~ 3.9 Ma), and 410 mbsf in Hole 1115C (~ 3.8 Ma).

DATA AND METHODS

The FMS tool is a four-pad microelectrical resistivity device that allows detailed investigation of vertical and lateral variations of formation resistivity (Bourke et al., 1989; Goodall et al., 1998). Schlumberger introduced the FMS tool in 1986. A slim version of this tool was designed in collaboration with the ODP Borehole Research Group at Lamont-Doherty Earth Observatory and was first used during Leg 126 (Pezard et al., 1992). The four pads produce an image that covers $\sim 25\%$ of the 25-cm-diameter borehole wall. Proper pad contact with the formation is ensured only where the borehole diameter is <37 cm. Formation resistivity is measured in 64 buttons: two rows of eight on each pad. Electrical current flows from the buttons into the formation and returns to the tool body. Current intensity variations in each button are proportional to the formation resistivity close to the borehole wall. Resistivity measurements are recorded every 2.5 mm, and the vertical resolution of the tool is of the order of 2.5 cm, although beds thinner than 2.5 cm can be detected if the resistivity contrast is high. The individual resistivity values are binned into color or grayscale classes to produce an image of the borehole wall.

F3. DPORO profiles hung on the mid- to upper Pliocene boundary, p. 15.



Formation resistivity depends primarily on the resistivity of the formation fluid, the connectivity of the pore space, and mineralogy. The high cation-exchange capacity of clay minerals generally leads to lower formation resistivity in clay-rich beds. In the largely unconsolidated sediments encountered at Woodlark Basin sites, the pixel tone of the images tends to be correlated with grain size, so that silt and sand beds and laminae show lighter tones and muddy sediments show darker tones. Where muds have a higher than average carbonate content, the resistivity increases and image tones are lighter (C  lerier et al., this volume). The FMS images from Holes 1118A, 1109D, and 1115C are generally of fair to good quality with data from at least one to two of the four pads on the tool (sufficient for mapping of bed boundaries). Locally poor contact of some of the pads with the borehole wall was the result of borehole rugosity caused by factors such as poor consolidation and caving.

The FMS images from the Pliocene turbidite succession at Sites 1118, 1109, and 1115 were printed at a scale of ~1:5 and interpreted side by side with conventional well logs and the detailed bed-by-bed descriptions and core photographs acquired during ODP Leg 180 (Taylor, Huchon, Klaus, et al., 1999). Bed-by-bed sedimentary sections (Fig. F4) were produced directly from the FMS images by picking the bases and tops of beds in the images. Gradational bed tops were positioned at the upper limit of the apparent grading, based on grayscale gradients from light (more resistive sand and coarse silt) to dark (more conductive claystone). Sharp tops of nongraded beds were recognized in some cases. Sand- and silt-bed thicknesses were then measured and tabulated in a spreadsheet file for each hole.

Three models have been advocated for the distribution of bed thicknesses in turbidite successions: a lognormal model (Ricci Lucchi, 1969), an exponential model (Drummond and Wilkinson, 1996), and a power-law model (Hiscott et al., 1992, 1993; Malinverno, 1997). Following a logarithmic transformation of bed thickness, data that are lognormally distributed should plot as a normal distribution with a "bell"-shaped frequency curve. Lognormal bed-thickness distributions characterize many sedimentary successions (Hinnov and Goldhammer, 1991; Drummond and Wilkinson, 1996).

If the data instead fit an exponential distribution, then the number of thin beds is much greater than the number of thick beds, there is no modal bed thickness, and the distribution is consistent with the following relationship:

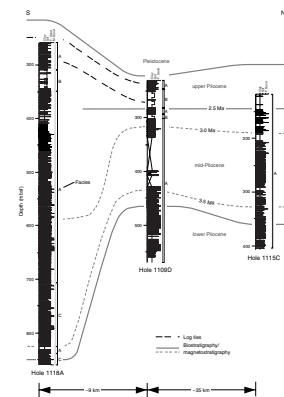
$$Y = ne^{-aT}, \quad (1)$$

where

- e = 2.71828,
- T = bed thickness,
- a = a constant,
- n = a constant, and
- Y = the number of beds thicker than T.

If a power-law distribution with a negative exponent characterizes a turbidite succession, then the number of thin beds is much greater than the number of thick beds. The power-law relationship is given by the following:

F4. Bed-by-bed columns based on FMS images, p. 16.



$$Y = nT^{-\beta}, \quad (2)$$

where n and T are defined above and β is a constant of order 1.0 given by the slope of a plot of Y vs. T in log-log space.

As a final step in the analysis of the Pliocene turbidite succession, the base of each turbidite bed at the three drill sites was assigned an absolute age using the age model of [Takahashi et al.](#) (this volume) and linear interpolation between picks on their accumulation-rate curves (Table T1). Then, bed number (starting with the deepest bed in each hole) was plotted against age to assess the frequency through time of turbidity currents reaching each of the three sites in the rift basin. The goal of this analysis was to discover (1) whether turbidity currents were focused into different parts of the basin at different times and (2) whether the number of sand and silt beds deposited per unit time was dramatically different from the basin axis to its northern margin.

RESULTS

Microresistivity Facies

Three log facies are recognized in the FMS images. Warping and contortion of bedding in Hole 1118A (280–285 and 320–330 mbsf) indicate slumping, but this deformation is so minor that we do not assign these deposits to an additional facies. The criteria used for facies recognition are the grain sizes and bed thicknesses of both sand–silt turbidites and intercalated muds. The grain sizes reported below are taken from handwritten shipboard core descriptions in the same intervals as the FMS images that characterize each facies. Because the images have a lower resolution than visual descriptions of cores, sedimentary structures could not be used to define log facies.

Facies A dominates the succession at Sites 1118, 1109, and 1115 (Fig. F4). It consists of graded beds of silt and very fine grained to medium-grained sand alternating with beds of silty to clayey mud (Fig. F5). The proportion of mud varies from ~35% to 80%; it is commonly moderately to intensely burrowed (Fig. F6C). In cores (Fig. F6) and FMS images, the sand and silt beds show sharp bases and gradational tops; a few beds have irregular scoured bases. Sand beds range in thickness from <5 to 50 cm, whereas silt beds are 10 to 100 cm thick.

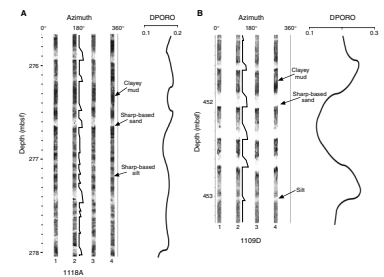
Facies B consists mostly of thick alternating intervals of silt and clayey mud; 5- to 20-cm-thick beds of sand are rare (~5%). The silt beds are 200 to 800 cm thick, and the clayey muds are 200 to 800 cm thick. Silt beds appear to be largely ungraded. Cores that sample the muds and some of the silts show bioturbation (Fig. F7). The silts are locally laminated.

Facies C is restricted to Site 1118, closest to the axis of the rift basin. It consists of interbedded very fine grained to medium-grained sands (~40%), silts (~30%), and clays (~30%). The greater sand content and coarser overall grain size of this facies are shown by the DPORO profile in Figure F3 from ~700 to 850 mbsf. The normally graded sands are mostly 5 to 80 cm thick, with rare graded beds 150 to 230 cm thick. These beds have sharp bases, gradational tops, local wavy to parallel laminations, and scattered mud clasts (Figs. F8, F9).

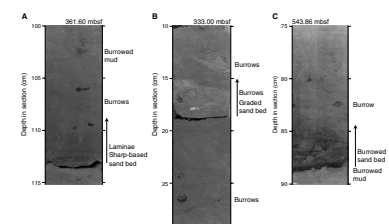
The graded silt and sand beds that characterize Facies A and C are interpreted as turbidity current deposits, consistent with the conclusions of shipboard scientists (Robertson et al., in press). The thick silt beds of

T1. Age picks constraining turbidite accumulation rates, p. 29.

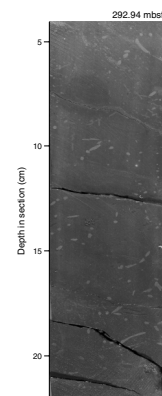
F5. FMS images of Facies A, p. 17.



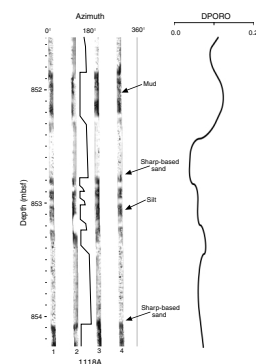
F6. Attributes of Facies A from cores, p. 19.



F7. Core photograph of Facies B, p. 21.



F8. FMS image showing thick-bedded sands of Facies C, p. 22.



Facies B are not believed to be turbidites. The widespread burrowing suggests that they are hemipelagic deposits that formed largely by rain-out from suspension. A similar depositional mechanism is inferred for the clayey muds of Facies B.

Bed-Thickness Distributions

Bed-thickness values for sand and silt turbidites were transformed to logarithms, binned into ~20 classes, and plotted as bar graphs (Fig. F10). These plots suggest that the bed-thickness populations are not lognormal—although there is a central mode, the populations are positively skewed with a long tail of particularly thick beds (Crowther, 2000). The tail of thicker beds is better accommodated by exponential and power-law models. At all sites, there is an approximately exponential decrease in frequency with increasing bed thickness, with a long tail of beds much thicker than the mode (Fig. F11).

Plots in log-log space of the number of beds thicker than T , vs. T , consist of segmented curves with one or more dominant linear trend (Fig. F12). These linear segments suggest power-law relationships, with β values (Equation 2) ranging from 1.4 to 5.6, but mostly <3.0. These β values are higher than for other turbidite successions (Hiscott et al., 1992, 1993; Pirmez et al., 1997) because the range in bed thickness is small (most beds <100 cm thick), even though the number of beds is large. In all plots, data points for $T < \sim 10$ cm deviate from a straight-line trend.

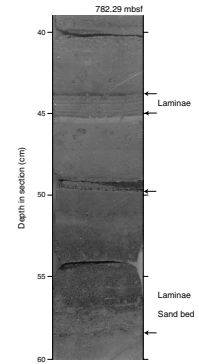
Turbidity-Current Frequencies

Plots of bed number vs. interpolated age for each site (Fig. F13) show some similarities but also striking differences across the asymmetric rift basin. Bathyal conditions (water >150 m deep) occurred first at Sites 1109 and 1115. The number of sand and silt turbidite beds that accumulated per million years rapidly reached ~930 at Site 1109 and ~440 at Site 1115 (recurrence intervals of 1075 and 2270 yr, respectively). These high turbidity-current frequencies persisted until at least 3.45 Ma at Site 1109 and 3.1 Ma at Site 1115. Because of a gap in the FMS data at Hole 1109D (Fig. F4), it is possible that both these sites continued to receive turbidites at high frequency until ~3.1 Ma. After ~3.1 Ma, the frequencies of turbidity current events were reduced at Sites 1109 and 1115 (respectively ~170 and ~70/m.y.; recurrence intervals = ~5,900 and ~14,300 yr).

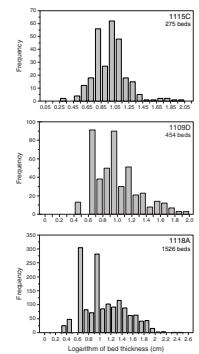
Site 1118 began to subside strongly by ~3.6 Ma, and until 3.45 Ma (or perhaps as late as ~3.2 Ma; see above) was receiving deposits of turbidity currents at the same rate as Site 1109 (Fig. F13). After that time, even though the frequency of depositing turbidity currents reaching Sites 1115 and 1109 decreased markedly, the frequency at Site 1118 remained high (~1500 beds/m.y.; recurrence interval = 670 yr). This continued until 2.6 Ma.

Between 2.6 and ~2.0 Ma, all sites recorded the arrival of turbidity currents at a sharply reduced rate as compared with rates that prevailed at 3.5 Ma. There was an increase in the frequency of turbidite deposition from 2.0 to 1.8 Ma at Sites 1109 and 1118. FMS data are not of sufficient quality in Hole 1115C to reveal the same increase, but cores deposited from 2.0 to 1.8 Ma at this site (~90–110 mbsf) are uniformly muddy, suggesting that it did not receive the same increased influx of turbidites.

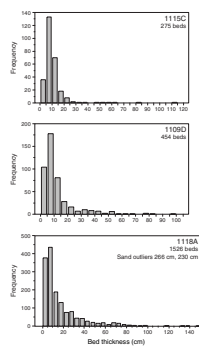
F9. Core photograph of Facies C, p. 23.



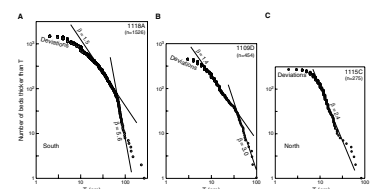
F10. Plots of lognormal tendency of bed-thickness distributions, p. 24.



F11. Plots showing exponential decline of bed thicknesses, p. 25.



F12. Logarithmic plots of the number of sand and silt beds thicker than T , vs. T , p. 26.



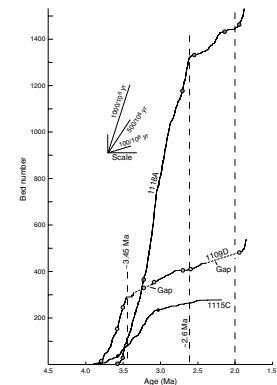
Discussion

In plots designed to reveal power-law tendencies in bed-thickness populations, the deviations in straight-line behavior for $T < 10$ cm (Fig. F12) may be the result of poor resolution of the very thinnest sand and silt beds in the FMS images, so that beds only a centimeter or so thick may have been missed. Alternatively, it is possible that the thinnest turbidites are mainly mud grade rather than consisting of silt or sand, so that they were not recognized or counted. Facies descriptions by the shipboard party (Taylor, Huchon, Klaus, et al., 1999) indicate that ~1-cm-thick beds are common, favoring the first alternative.

The segmented nature of these graphs for $T > 10$ (Fig. F12) can be explained using suggestions published by Malinverno (1997). He shows that natural bed-thickness data sets can be expected to plot as segmented linear trends with different slopes (i.e., different β values, Equation 2) if there is a relationship between bed length and bed thickness that depends on the bed volume. For example, smaller flows and their deposits might be confined by topographic features in the basin (e.g., channels or subdued depositional topography), whereas larger flows might be free to spread over wider areas (Rothman and Grotzinger, 1995; Malinverno, 1997). In this case, the β value would be greatest for the thicker beds (larger flows), just as in Figure F12. Multichannel seismic profiles between Sites 1118 and 1109 show a broad north–northwest-trending trough (paleochannel) at the level of a widespread erosional surface situated below the Pliocene turbidite succession (Goodliffe et al., 1999). Site 1109 was drilled in this trough and Site 1118 along its flank. Confinement of turbidity currents by such underlying topography might have prevented the free spreading of flows across the floor of the rift basin, thus accounting for the segmented nature of bed-thickness plots. Channels with smaller dimensions (<10 m depth) might also have been present but are unresolved in the multi-channel seismic data.

The Woodlark Basin is a site of active rifting and profound subsidence, where earthquakes are potentially responsible for triggering turbidity currents and other sediment gravity flows (e.g., silt-laden liquefied flows or debris flows) like those that generated the Pliocene basinal succession. Earthquake magnitudes typically follow power-law distributions (Turcotte, 1989); hence, earthquakes have been proposed as a triggering mechanism for turbidity currents whose deposits likewise conform to power-law distributions (Hiscott et al., 1993; Beattie and Dade, 1996). According to Kuribayashi and Tatsuoka (1977) and Keefer (1984), earthquakes with magnitudes of >5.0 are required to cause significant liquefaction for the initiation of sediment gravity flows. As the distance from the epicenter increases, so does the minimum magnitude required for liquefaction, so that a magnitude 7.0 shock can liquefy sediment as far as ~100 km from the epicenter. The bed-thickness data sets from Holes 1118A, 1109D, and 1115C are broadly consistent with power-law behavior, so that seismic triggering is a possible explanation for the genesis of sediment gravity flows during the late early Pliocene to late Pliocene. Turbidity-current recurrence intervals of ~1000 yr to several thousands of years (Fig. F13) are similar to those determined for thin-to medium-bedded turbidites from the Izu-Bonin forearc basin by Hiscott et al. (1992, 1993), another area with strong seismic activity. Hiscott et al. (1992, 1993) found these recurrence intervals for turbidites to be one to two orders of magnitude greater than the recurrence intervals for large-magnitude earthquakes

F13. Plots of turbidite bed number vs. the age of the base of each bed, p. 27.

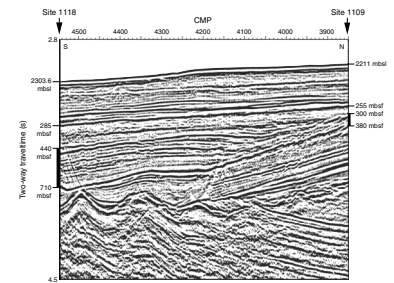


in the subduction zones of the western Pacific. A Web-based search (www.neic.cr.usgs.gov/neis/epic/epic_rect.html) of the number of earthquakes of magnitude ≥ 4.0 since 1973 in two areas, one south of Japan (33° – 35° N, 135° – 139° E) and the other in the source area for the Woodlark Basin (8° – 10° S, 150° – 153° E), identified 389 and 78 events, respectively. Hence, seismic events are less frequent in the rift setting than above subduction zones by a factor of ~ 5 , and depositing turbidity currents are estimated to occur ~ 0.5 – 1.5 orders of magnitude less frequently than potential seismic triggers. One must imagine that the availability of seismic triggers is not alone sufficient to generate turbidity currents; in addition, failures large enough to initiate far-traveled turbidity currents must only occur after an extended period of deposition on basin slopes to accumulate the unstable mass that eventually fails (Hiscott et al., 1993).

The sandiest and thickest turbidites accumulated along the more subsident basin axis, as shown by the relative concentration of sand-prone deposits at the more southerly Site 1118 (Fig. F4). Seismic data confirm that a wedge of deposits at Site 1118 (500–750 mbsf) thins dramatically at the margin of the central trough of the basin so that equivalent deposits are attenuated at Site 1109 (300–400 mbsf) (Fig. F14). Even within the turbidite succession at Site 1118, some intervals are more sandy than others, consisting of stacked deposits of Facies C, forming sand-bed clusters (cf. Chen and Hiscott, 1999a). Statistical analysis using procedures of Chen and Hiscott (1999b) shows no vertical trends in bed thickness in these sand-bed clusters (Bidgood, 2000). We interpret these clusters to be the result of pulses of source-area uplift at the basin margins or pulses in the rate of relative sea-level change, with the timing of sediment delivery into the deep basinal areas modulated by earthquakes. According to Kennett and Hodell (1995), global sea level fell ~ 25 – 30 m from the middle to late Pliocene. Irregular steps in the pace of this sea level fall might account for variable rates of sand shedding from the source region.

From the axial area (Site 1118) to the northern margin of the rift basin (Site 1115) (Fig. F2), the number of turbidites deposited per unit time seems to decrease, particularly after 3.45 Ma (Fig. F13). There may be a real difference in the number of turbidity currents that reached each site, perhaps because the more subsident areas near the basin axis remained deeper than the rest of the rift, encouraging a greater number of gravity flows to seek out the axial area (e.g., Fig. F14). Alternatively, the number of depositional events may have been similar across the rift basin. This would be consistent with Figure F13 only if the coarser sandy and silty turbidite divisions (recognizable in FMS images and cores) tended to accumulate near Site 1118, whereas the other two sites received deposits of mainly turbidite mud from the distal fringes of the same flow events. Although the number of turbidites counted in the FMS images from Hole 1115C is only about 15% of the number counted in Hole 1118A, the stratigraphic thickness at Site 1115 is 50% the thickness of the time-equivalent succession at Site 1118 (Fig. F3). This must reflect a high rate of mud deposition at Site 1115 to compensate for the lack of sandy and silty turbidites. We interpret this rapidly deposited mud to indeed be the result of deposition from turbidity currents that dropped their sand load closer to the basin axis. Thin mud turbidites are difficult to distinguish from hemipelagic mudstones, particularly if much of the sediment is bioturbated as at Sites 1115 and 1109 (Robertson et al., in press). Very thin mud turbidites might also not be preserved because of erosion beneath subsequent flows.

F14. Multichannel seismic profile between Sites 1118 and 1109, p. 28.



Sites 1118, 1109, and 1115 run south to north (Fig. F2), and facies, interpreted from both cores and FMS images, indicate a fining and thinning trend toward the north for the entire turbidite succession. The main provenance for the turbidite sands and silts, however, is to the west in the vicinity of the Papuan Peninsula and D'Entrecasteaux Islands (Figs. F1, F2). Turbidity currents presumably entered the rift basin from its western end and then flowed axially toward the east. Most turbidity currents likely sought out the deeper axis of the rift, particularly after ~3.45–3.1 Ma when the present basin axis (closest to Site 1118) began to subside more rapidly than the northern basin margin (Sites 1109 and 1115).

CONCLUSIONS

1. Microresistivity (FMS) images collected along a transect of three ODP drill sites in the western Woodlark Basin confirm and complement shipboard descriptions of the thin-bedded turbidite succession that accumulated from the late early Pliocene to early late Pliocene (3.9–1.8 Ma). Based mainly on sand-bed and silt-bed thicknesses, as well as percentages of interbedded mud, the FMS images have been divided into three microresistivity facies. Only Facies C contains clusters of thick sand beds; it is confined to the southern Site 1118.
2. Thickness distributions of turbidite beds are broadly exponential (many thin beds and few thick beds) but also approximate power-law distributions with either one or two linear segments (i.e., one or two β values for different ranges of bed thickness). These patterns can be interpreted to result from partial confinement of less voluminous flows in the rift basin, perhaps because of subtle seabed topography and/or channels. Broad conformity with a power-law model is consistent with triggering of turbidity currents by earthquakes in the tectonically active rift.
3. Frequencies of turbidites reach ~930 beds/m.y. at Sites 1109 and 1118 in the period 3.6–3.45 Ma (beginning somewhat early at Site 1109). Subsequently, frequencies drop at Sites 1109 and 1115 but remain unchanged at Site 1118 until ~2.6 Ma. This apparent higher rate of arrival of turbidity currents closest to the basin axis may indicate (a) greater trapping of bottom-hugging gravity flows in the morphologically deeper axial trough or (b) frequent deposition of only mud from distal turbidity currents once they had traveled beyond the axial zone of the rift.

ACKNOWLEDGMENTS

We thank the crew of the *JOIDES Resolution* for skillful operations in the Woodlark Basin. This research used samples and/or data provided by the Ocean Drilling Program (ODP). ODP is sponsored by the U.S. National Science Foundation (NSF) and participating countries under management of Joint Oceanographic Institutions (JOI), Inc. Funding for this research was provided by a Natural Sciences and Engineering Research Council of Canada grant to R.N.H. and by undergraduate scholarships to M.B. and T.E.C. from the Canadian ODP Secretariat. Funds to cover travel expenses for S.A.A. to participate in Leg 180 were generously provided by the Canadian ODP Secretariat and by the Deans

of both Science and Graduate Studies at Memorial University of Newfoundland. R.N.H. thanks the Leg 180 co-chief scientists and the shipboard party for granting all three junior authors (as nonshipboard scientists) access to primary data within the moratorium period. Critical comments by reviewers Carlos Pirmez and Philippe Pezard improved the content and organization of the paper.

REFERENCES

- Beattie, P.D., and Dade, W.B., 1996. Is scaling in turbidite deposition consistent with forcing by earthquakes? *J. Sediment. Res.*, 66:909–915.
- Bidgood, M., 2000. Cyclicity of Pliocene rift-basin turbidites, Woodlark Basin, from FMS borehole images (ODP Leg 180) [Hon. B.S. thesis]. Memorial Univ., St. John's, Newfoundland, Canada.
- Bourke, L., Delfiner, P., Trouiller, J.-C., Fett, T., Grace, M., Luthi, S., Serra, O., and Standen, E., 1989. Using Formation MicroScanner images. *Tech. Rev.*, 37:16–40.
- Chen, C., and Hiscott, R.N., 1999a. Statistical analysis of facies clustering in submarine-fan turbidite successions. *J. Sediment. Res.*, 69:505–517.
- , 1999b. Statistical analysis of turbidite cycles in submarine fan successions: tests for short-term persistence. *J. Sediment. Res.*, 69:486–504.
- Crowther, T.E., 2000. Bed-thickness statistics for Pliocene rift-basin turbidites, Woodlark Basin, from FMS borehole images (ODP Leg 180) [Hon. B.S. thesis]. Memorial Univ., St. John's, Newfoundland, Canada.
- Drummond, C.N., and Wilkinson, B.H., 1996. Strata thickness frequencies and the prevalence of orderedness in stratigraphic sequences. *J. Geol.*, 104:1–18.
- Goodall, T.M., Møller, N.K., and Rønningsland, T.M., 1998. The integration of electrical image logs with core data for improved sedimentological interpretation. In Harvey, P.K., and Lovell, M.A. (Eds.), *Core-Log Integration*. Spec. Publ.—Geol. Soc. London, 136:237–248.
- Goodliffe, A.M., Taylor, B., and Martinez, F., 1999. Data report: Marine geophysical surveys of the Woodlark Basin region. In Taylor, B., Huchon, P., Klaus, A., et al., *Proc. ODP, Init. Repts.*, 180, 1–20 [CD-ROM]. Available from: Ocean Drilling Program, Texas A&M University, College Station, TX 77845-9547, U.S.A.
- Hinnov, L.A., and Goldhammer, R.K., 1991. Spectral analysis of the middle Triassic Latemar limestone. *J. Sediment. Petrol.*, 61:1173–1193.
- Hiscott, R.N., Colella, A., Pezard, P., Lovell, M.A., and Malinverno, A., 1992. Sedimentology of deep-water volcanoclastics, Oligocene Izu-Bonin forearc basin, based on formation microscanner images. In Taylor, B., Fujioka, K., et al., *Proc. ODP, Sci. Results*, 126: College Station, TX (Ocean Drilling Program), 75–96.
- , 1993. Basin-plain turbidite succession of the Oligocene, Izu-Bonin, intra-oceanic forearc basin. *Mar. Pet. Geol.*, 10:450–466.
- Keefer, D.K., 1984. Landslides caused by earthquakes. *Geol. Soc. Am. Bull.*, 95:406–421.
- Kennett, J.P., and Hodell, D.A., 1995. Stability or instability of Antarctic ice sheets during warm climates of the Pliocene? *GSA Today*, 5:1, 10–13, 22.
- Kuribayashi, E., and Tatsuoka, F., 1977. History of earthquake-induced soil liquefaction in Japan. *Bull. Public Works Res. Inst. (Jpn. Min. Construction)*, 31:1–26.
- Malinverno, A., 1997. On the power-law size distribution of turbidite beds. *Basin Res.*, 9:263–274.
- Pezard, P.A., Lovell, M.A., and Hiscott, R.N., 1992. Downhole electrical images in volcanoclastic sequences of the Izu-Bonin forearc basin, western Pacific. In Taylor, B., Fujioka, K., et al., *Proc. ODP, Sci. Results*, 126: College Station, TX (Ocean Drilling Program), 603–624.
- Pirmez, C., Hiscott, R.N., and Kronen, J.D., Jr., 1997. Sandy turbidite successions at the base of channel-levee systems of the Amazon Fan revealed by FMS logs and cores: unraveling the facies architecture of large submarine fans. In Flood, R.D., Piper, D.J.W., Klaus, A., and Peterson, L.C. (Eds.), *Proc. ODP, Sci. Results*, 155: College Station, TX (Ocean Drilling Program), 7–33.
- Ricci Lucchi, F., 1969. Channelized deposits in the middle Miocene flysch of Romagna (Italy). *G. Geol.*, 36:203–282.
- Robertson, A.H.F., Awadallah, S.A.M., Gerbaudo, S., Lackschewitz, K.S., Monteleone, B.D., Sharp, T.R., and the ODP Leg 180 Shipboard Scientific Party, in press. Evolu-

- tion of the Miocene-Recent Woodlark Rift Basin, SW Pacific, inferred from sediments drilled during Ocean Drilling Program Leg 180. In Wilson, R.C.L., Froitzheim, N., Taylor, B., and Whitmarsh R.B. (Eds.), *Non-Volcanic Rifting of Continental Margins: A Comparison of Evidence from Land and Sea*. Spec. Publ.—Geol. Soc. London, 187. [N1]
- Rothman, D.H., and Grotzinger, J.P., 1995. Scaling properties of gravity-driven sediments. *Nonlinear Processes in Geophys.*, 2:178–185.
- Shipboard Scientific Party, 1995. Explanatory notes. In Flood, R.D., Piper, D.J.W., Klaus, A., et al., *Proc. ODP, Init. Repts.*, 155: College Station, TX (Ocean Drilling Program), 47–81.
- , 1999. Explanatory notes. In Taylor, B., Huchon, P., Klaus, A., et al., *Proc. ODP, Init. Repts.*, 180, 1–75 [CD-ROM]. Available from: Ocean Drilling Program, Texas A&M University, College Station, TX 77845-9547, U.S.A.
- Taylor, B., Goodliffe, A.M., and Martinez, F., 1999. How continents break up: insights from Papua New Guinea. *J. Geophys. Res.*, 104:7497–7512.
- Taylor, B., Huchon, P., Klaus, A., et al., 1999. *Proc. ODP, Init. Repts.*, 180 [CD-ROM]. Available from: Ocean Drilling Program, Texas A&M University, College Station, TX 77845-9547, U.S.A.
- Turcotte, D.L., 1989. Fractals in geology and geophysics. *Pure Appl. Geophys.*, 131:171–196.

Figure F1. Regional setting of the Woodlark Basin. The lightly shaded and outlined area in the east corresponds to new oceanic crust formed following plate separation; in the west (area of Fig. F2, p. 14), the rift is still floored by older crust. Bold arrows indicate Pliocene sediment transport routes (Robertson et al., in press).

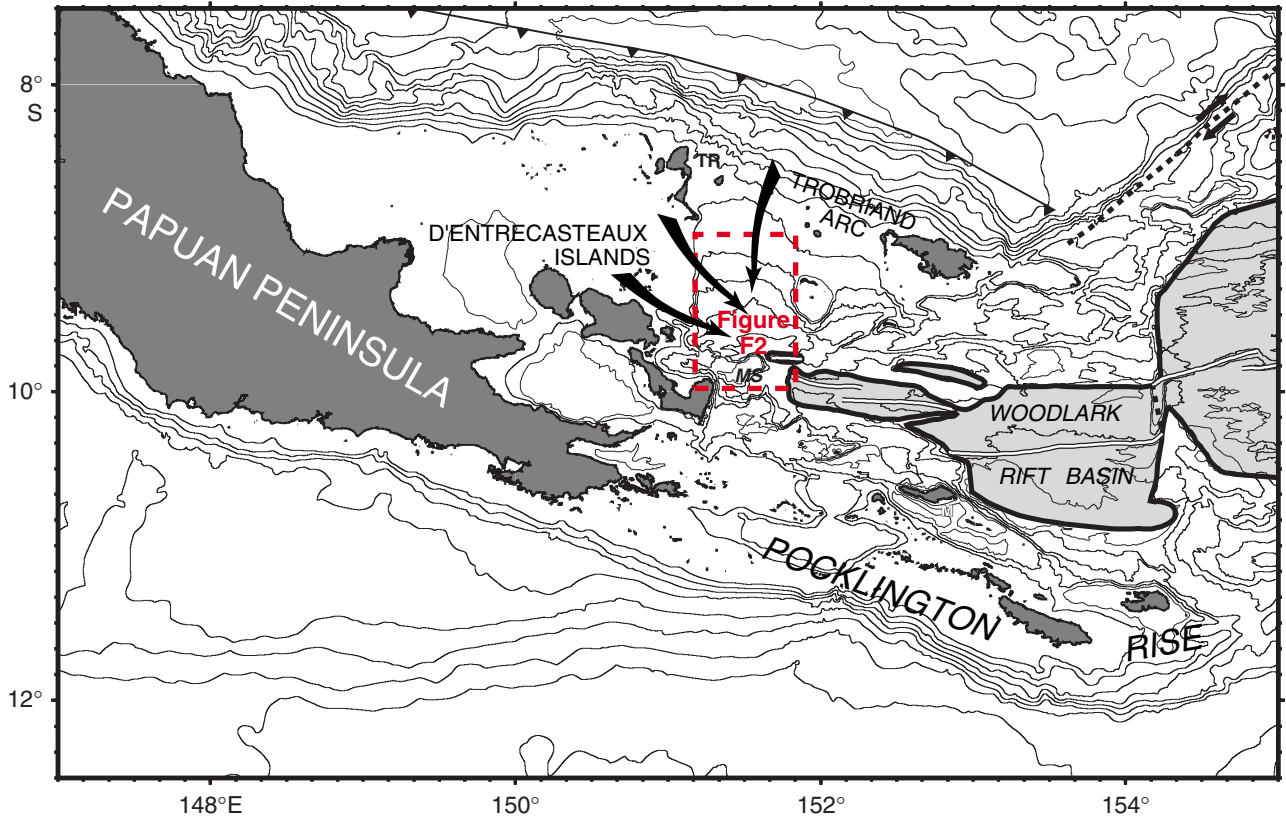


Figure F2. Location of ODP sites around and north of the Moresby Seamount (MS). Sites 1118, 1109, and 1115 are the focus of this paper. The bathymetric contour interval is 200 m; contours are labeled each kilometer of water depth. Bold lines with tick marks indicate the main normal faults and their direction of dip (from Taylor et al., 1999). Large arrows indicate sediment transport routes during the Pliocene (Robertson et al., in press).

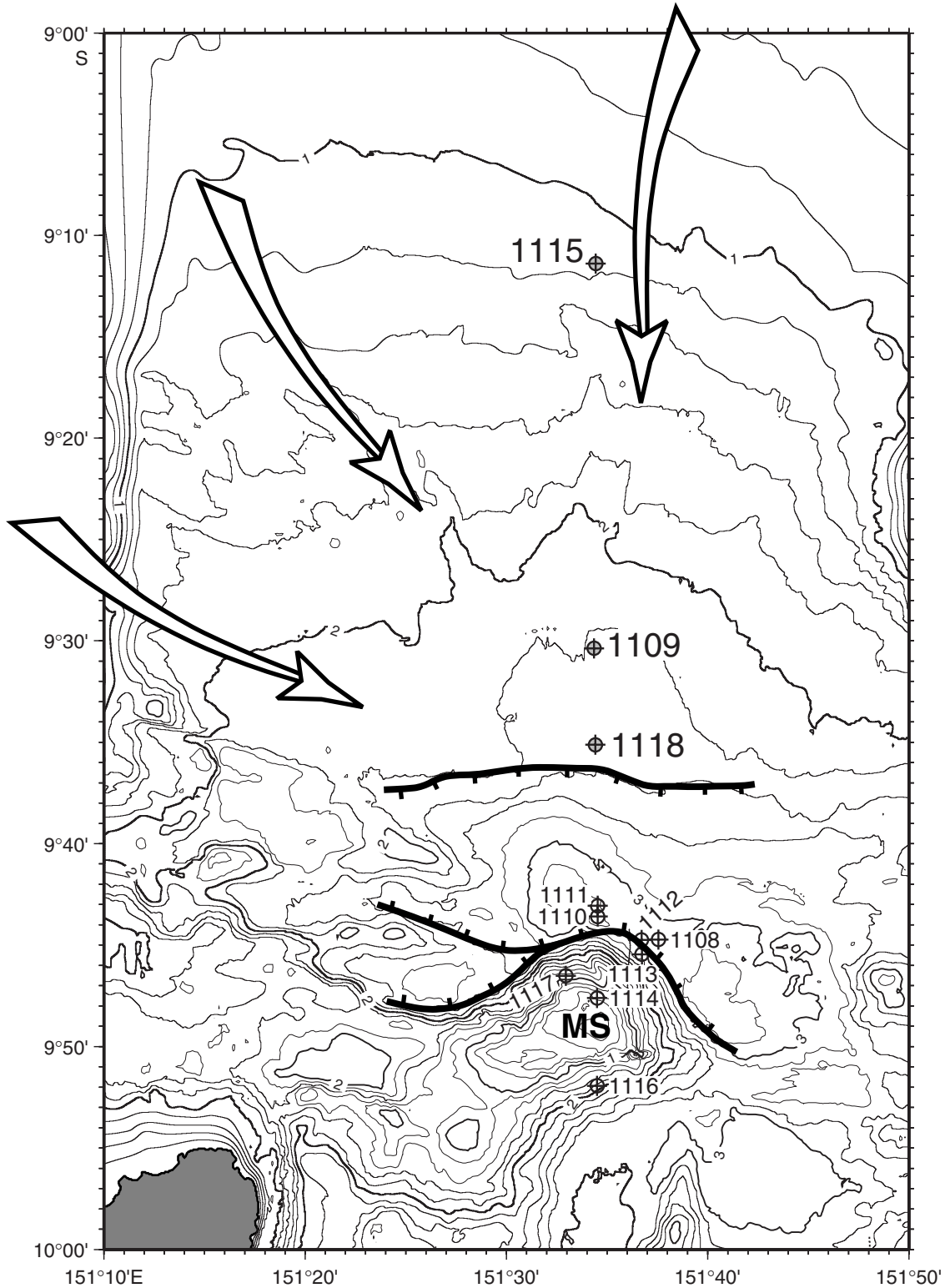


Figure F3. DPORO profiles hung on the mid- to upper Pliocene boundary and correlated using age ties from Takahashi et al. (this volume). Calculation of DPORO is explained by C  lerier et al. (this volume). Figure F4, p. 16, shows FMS-based bed-by-bed sections plotted on the same correlation template.

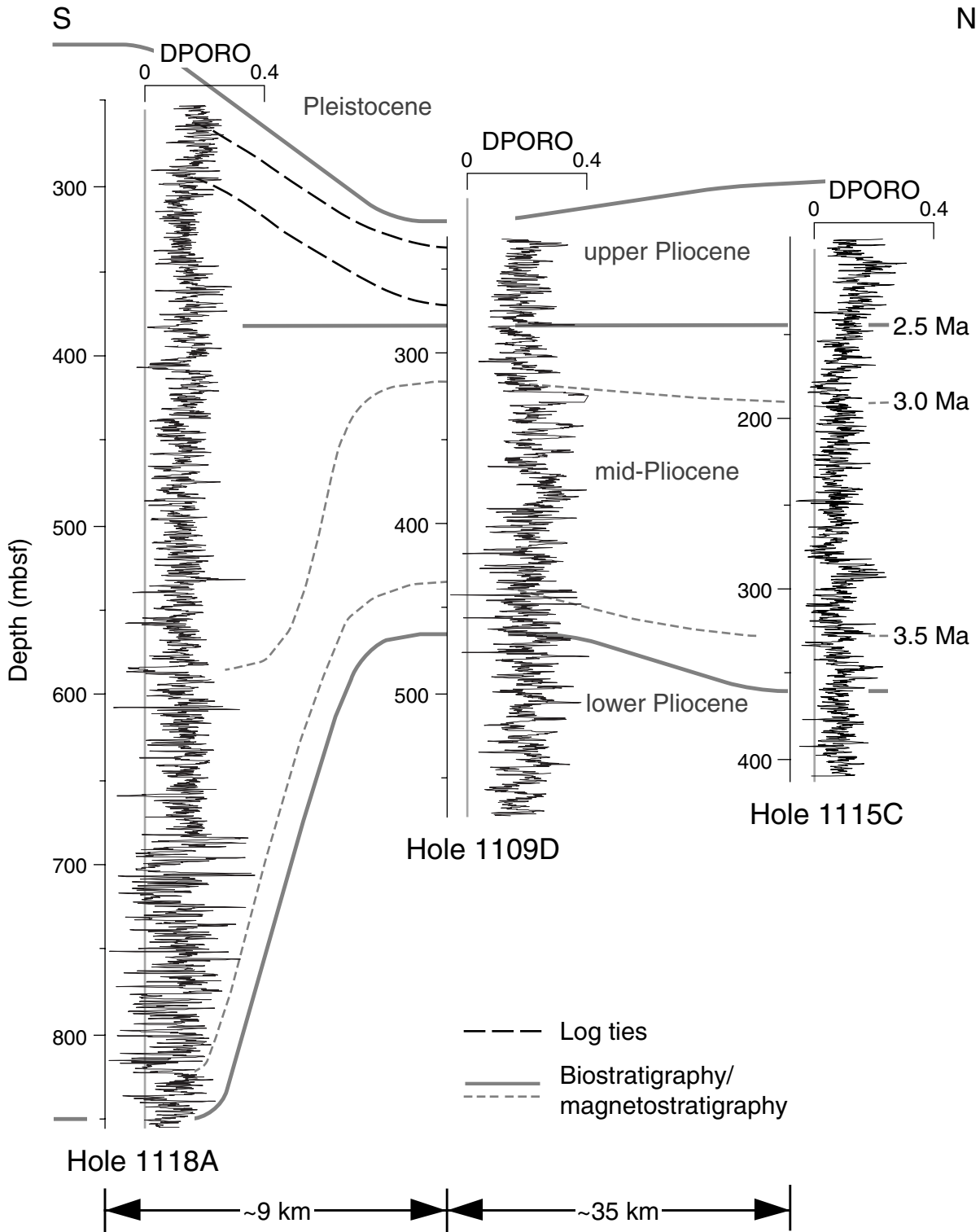


Figure F4. Bed-by-bed columns based on FMS images. Correlation is identical to Figure F3, p. 15, and is based on age ties from Takahashi et al. (this volume). Turbidite sands in Hole 1118A are thicker and more abundant than in other holes, particularly below ~700 mbsf. Facies letters are provided adjacent to the columns. Very fine grained sand could not be distinguished from silt and fine-grained sand on the FMS images, so is not recognized as a separate sediment grade. (This figure is available in an **oversized format.**)

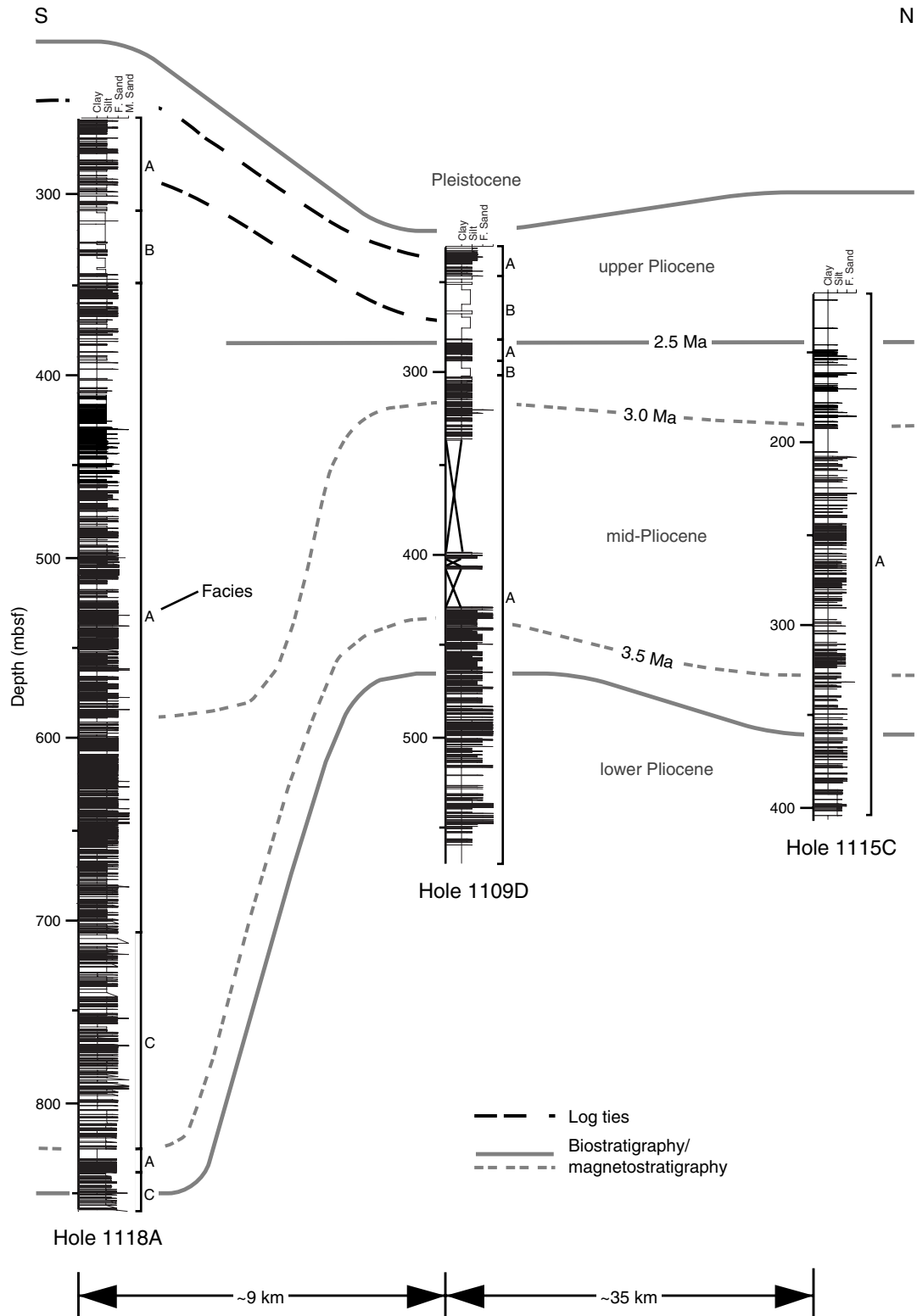


Figure F5. FMS images of Facies A. The four strip images are located at right angles to one another around the borehole wall and follow the track taken by each spring-loaded pad as it was pulled up the open hole. Pseudo-weathering profiles between the images for pads 2 and 3 indicate relative grain-size variations. DPORO values are extracted from Figure F3, p. 15, and indicate greater clay content with higher values (C  lerier et al., this volume). **A.** Thin- to medium-bedded graded beds of sand and silt (Hole 1118A; 275.7–278.1 mbsf). **B.** Thin- to medium-bedded graded sands (Hole 1109D; 451.3–453.3 mbsf). (Figure shown on next page.)

Figure F5 (continued). (Caption shown on previous page.)

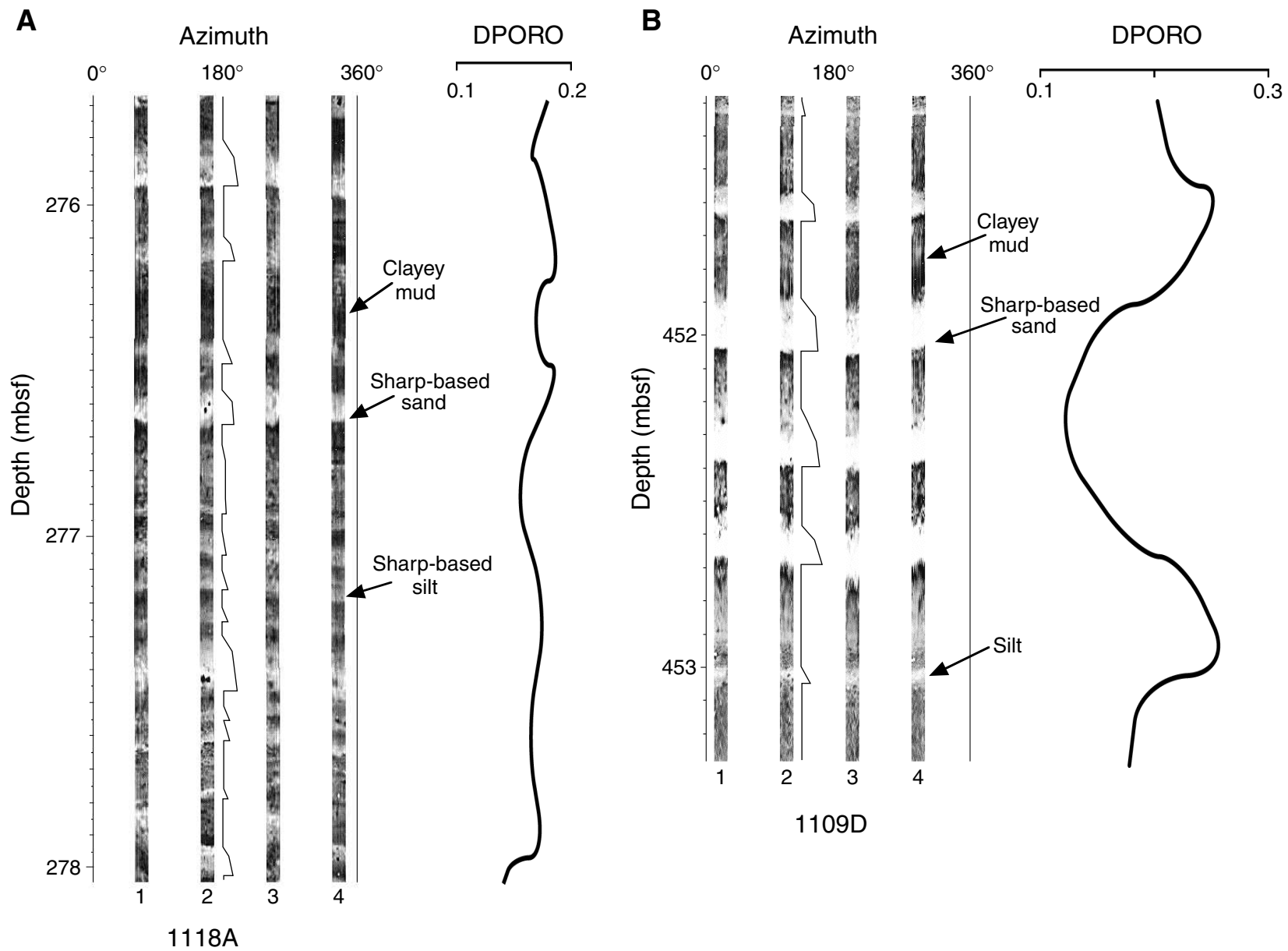


Figure F6. Attributes of Facies A from cores. Vertical arrows indicate the extent of graded sand beds. **A.** A sharp-based, graded, medium-grained to very fine grained sand with lower planar laminae from 108 to 113 cm (interval 180-1109D-2R-2, 100–115 cm; 361.60–361.75 mbsf). The remainder of the photograph shows bioturbated silty mud with sand-filled burrows. **B.** A turbidite (15–19 cm) that grades from very fine grained sand to silt and is burrowed at its top (interval 180-1115C-6R-2, 10–29 cm; 333.00–333.19 mbsf). The base of this turbidite may have been ground away during rotary coring, and therefore the bed may have been both thicker and coarser at its base. The remainder of the interval consists of bioturbated silty clay with sand-filled burrows and scattered foraminifers. Arcuate scratches from 20 to 25 cm are saw marks. **C.** A sharp-based, graded, medium-grained to very fine grained sand from 84 to 89 cm (interval 180-1109D-21R-2, 76–90 cm; 543.86–544.00 mbsf). Burrowers have mixed the sand with the interbedded silty clay, so that there are clay-filled burrows in the sandy turbidite and sand-filled burrows elsewhere. The silty clay contains foraminifer tests and shell fragments. ([Figure shown on next page.](#))

Figure F6 (continued). (Caption shown on previous page.)

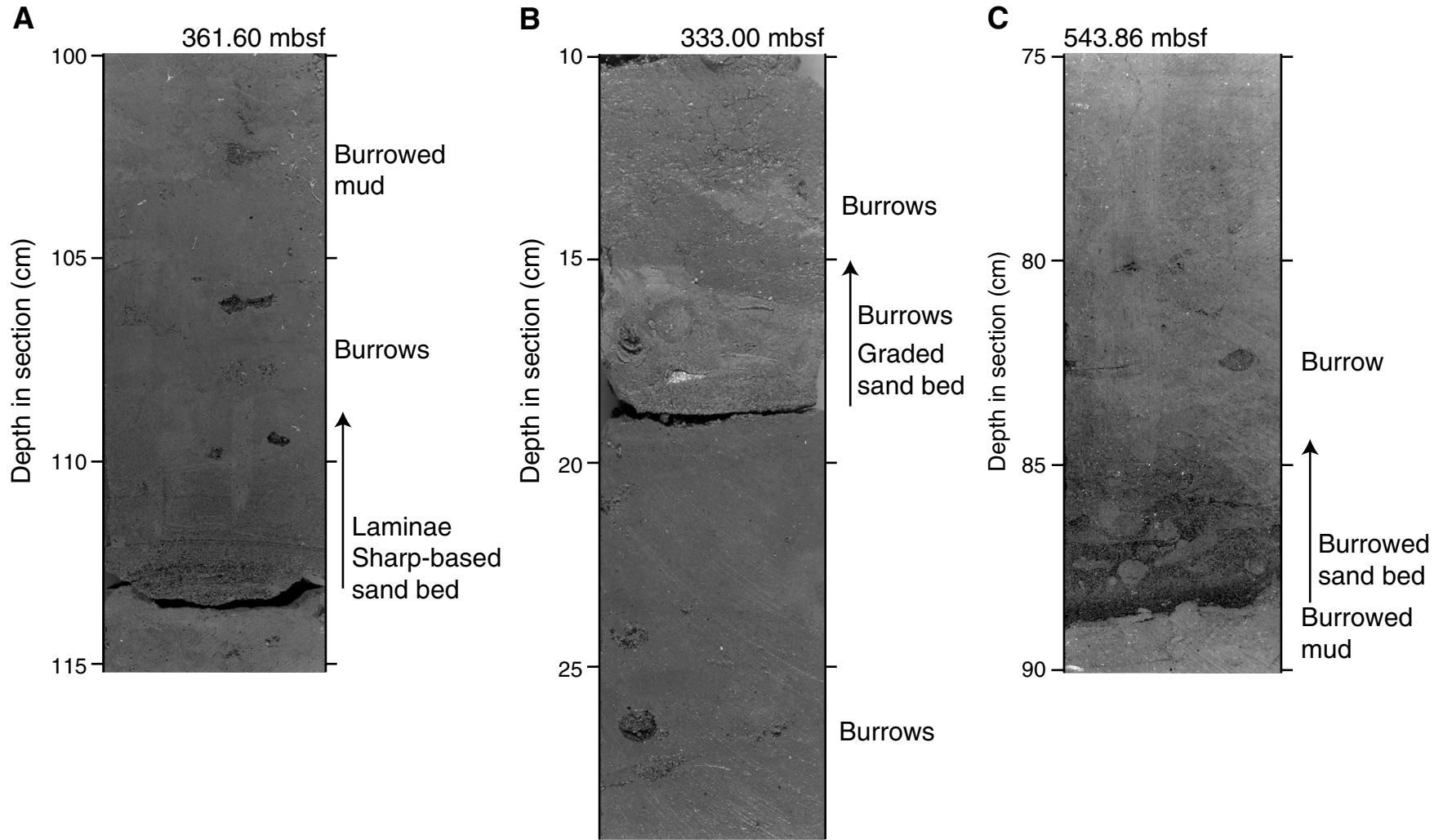


Figure F7. Core photograph of Facies B (interval 180-1118A-10R-2, 4–22 cm; 292.94–293.12 mbsf) showing structureless silty mud with *Chondrites* burrows. *Zoophycos* is also common in Facies B. Arcuate scratches from 4 to 7 cm are saw marks.

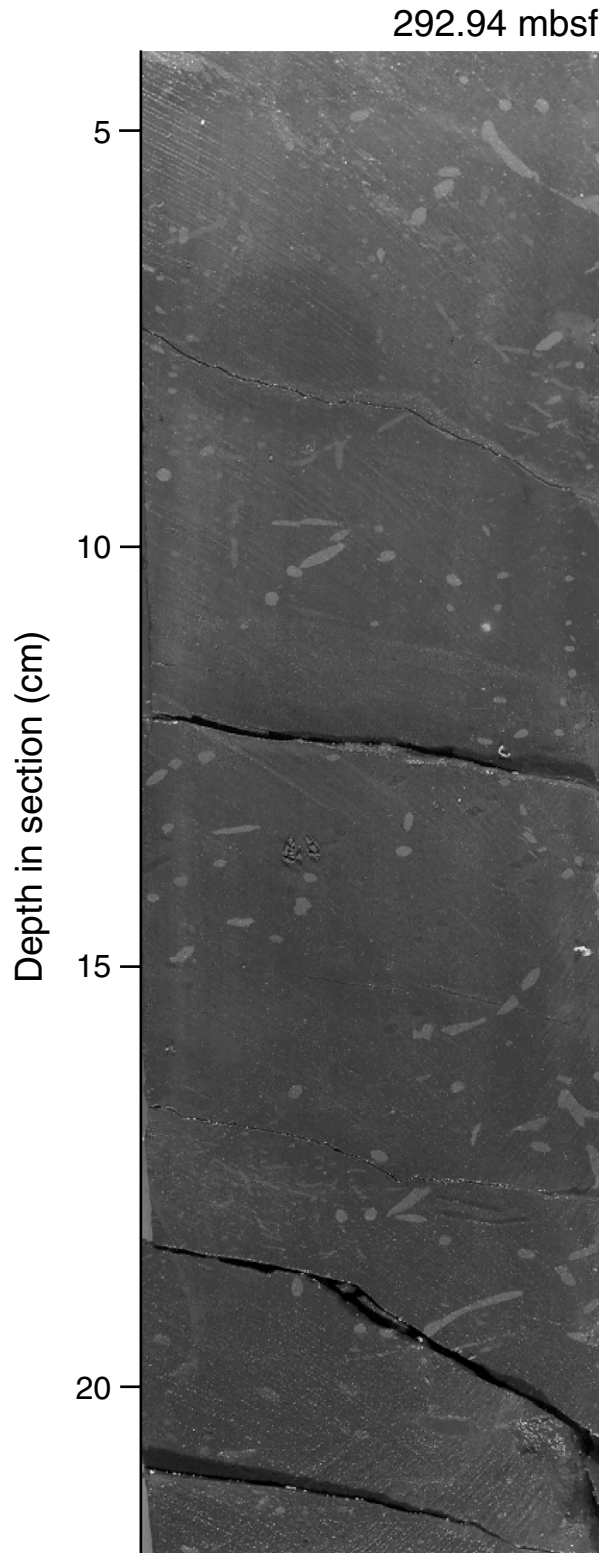


Figure F8. FMS image showing thick-bedded sands of Facies C (Hole 1118A; 843.3–846.0 mbsf). This image is fuzzy because the borehole wall is irregular in these friable sands, leading to locally poor contact of the spring-loaded pads. The silts and muds may simply be the finer-grained tops of the sand-prone turbidites or may, in part, consist of thin silty turbidite interbeds. The four strip images are located at right angles to one another around the borehole wall and follow the track taken by each spring-loaded pad as it was pulled up the open hole. A pseudo-weathering profile between the images for pads 2 and 3 indicates relative grain-size variations. DPORO values are extracted from Figure F3, p. 15, and indicate greater clay content with higher values (C  lerier et al., this volume). Note that DPORO values are all higher than those in Figure F5, p. 17.

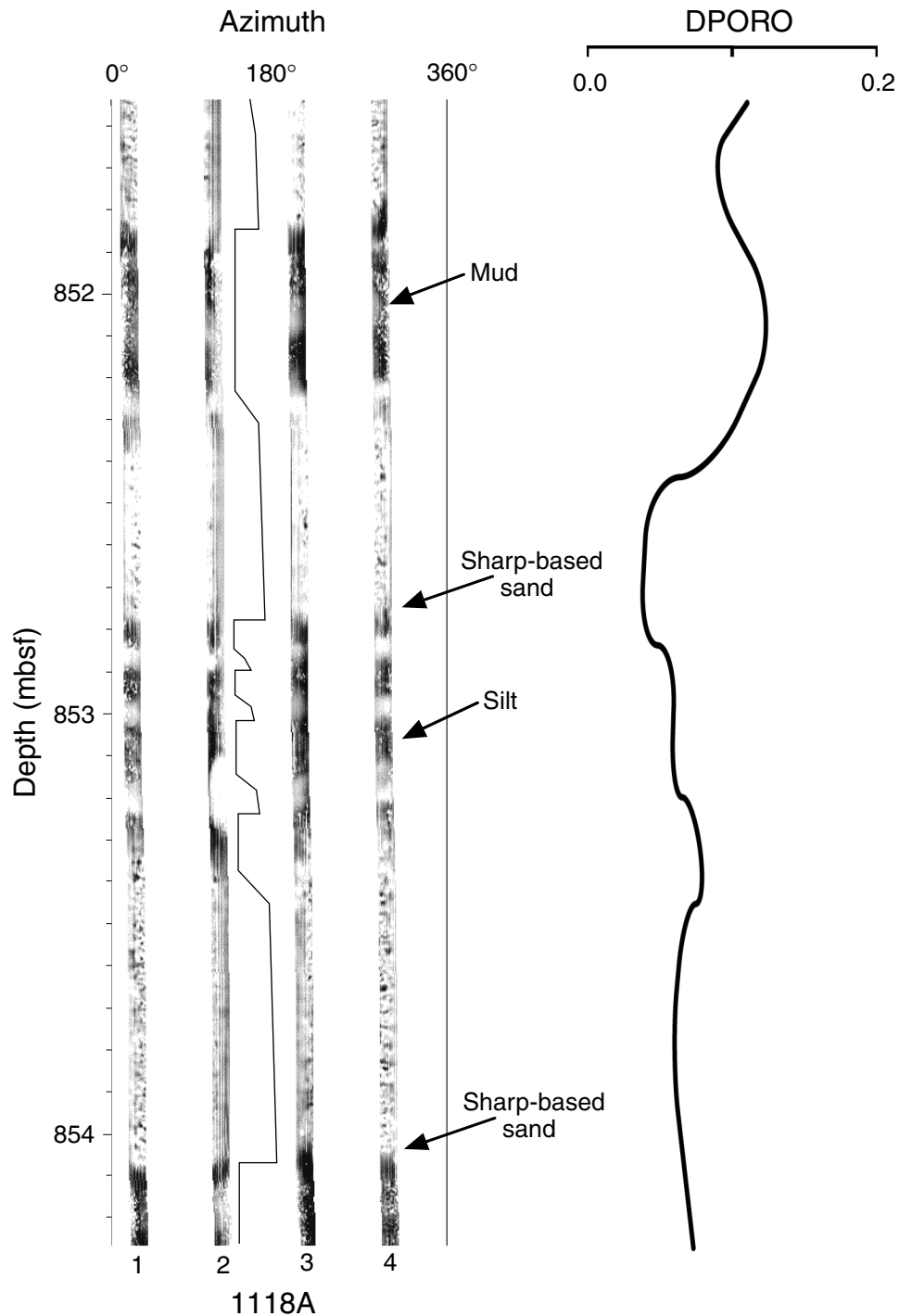


Figure F9. Core photograph of Facies C (interval 108-1118A-61R-1, 39–60 cm; 782.29–782.50 mbsf) showing four graded, sandy turbidites with arrows indicating their bases. The lowest bed contains small mud clasts (~1–2 mm in size) and is medium grained at its base. Parallel laminae are present from 43.5 to 45 and 55 to 58 cm. All sand beds are slightly burrowed. Arcuate scratches at 43, 50, and 58–60 cm are saw marks.

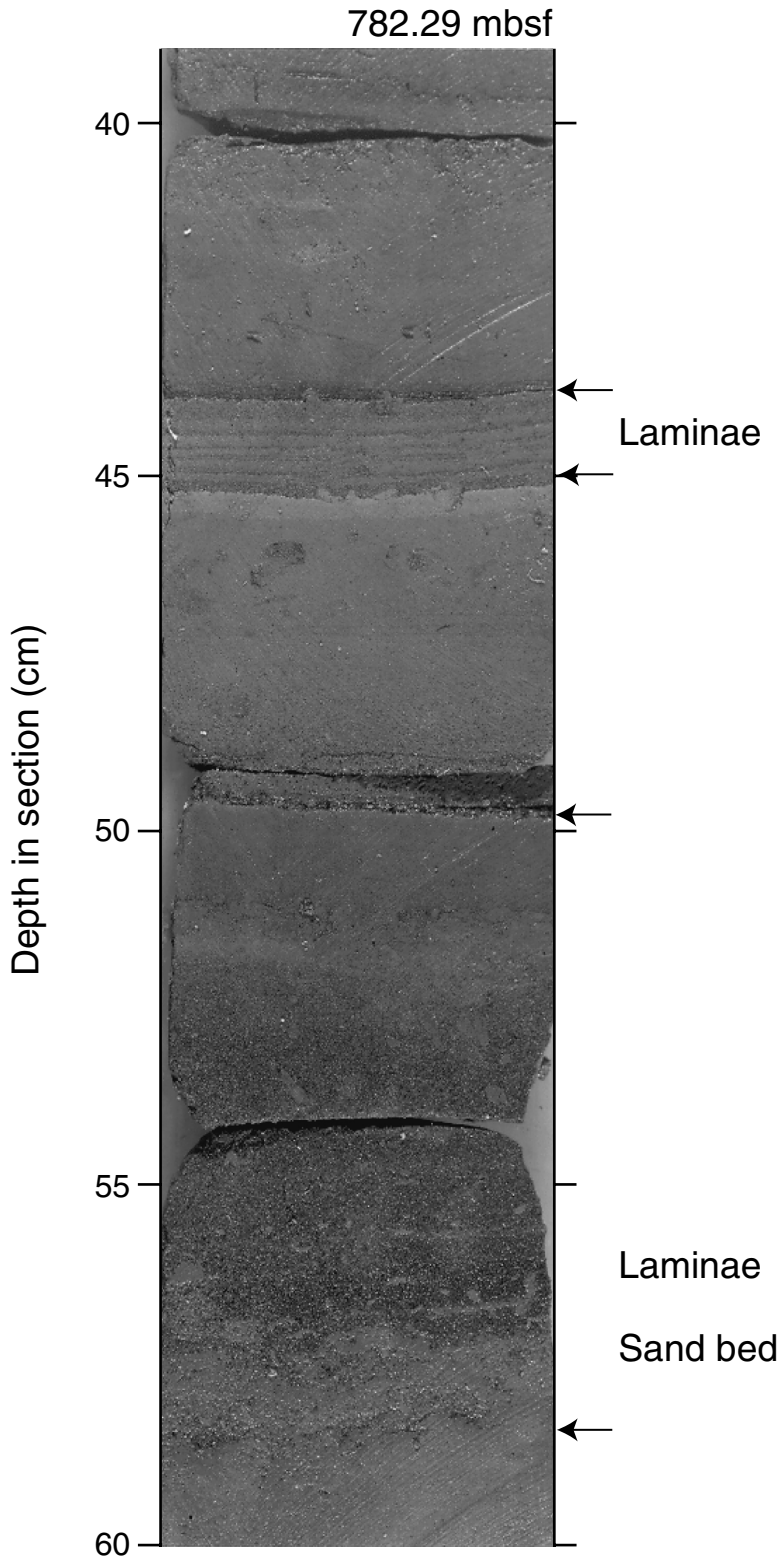


Figure F10. Plots showing the lognormal tendency of bed-thickness distributions for Pliocene silt and sand turbidites from Holes 1118A, 1109D, and 1115C. Values on the x-axis are powers of 10 (e.g., the bar between 0.6 and 0.7 shows the number of beds with thickness between $10^{0.6}$ and $10^{0.7}$ cm, or 3.98–5.01 cm).

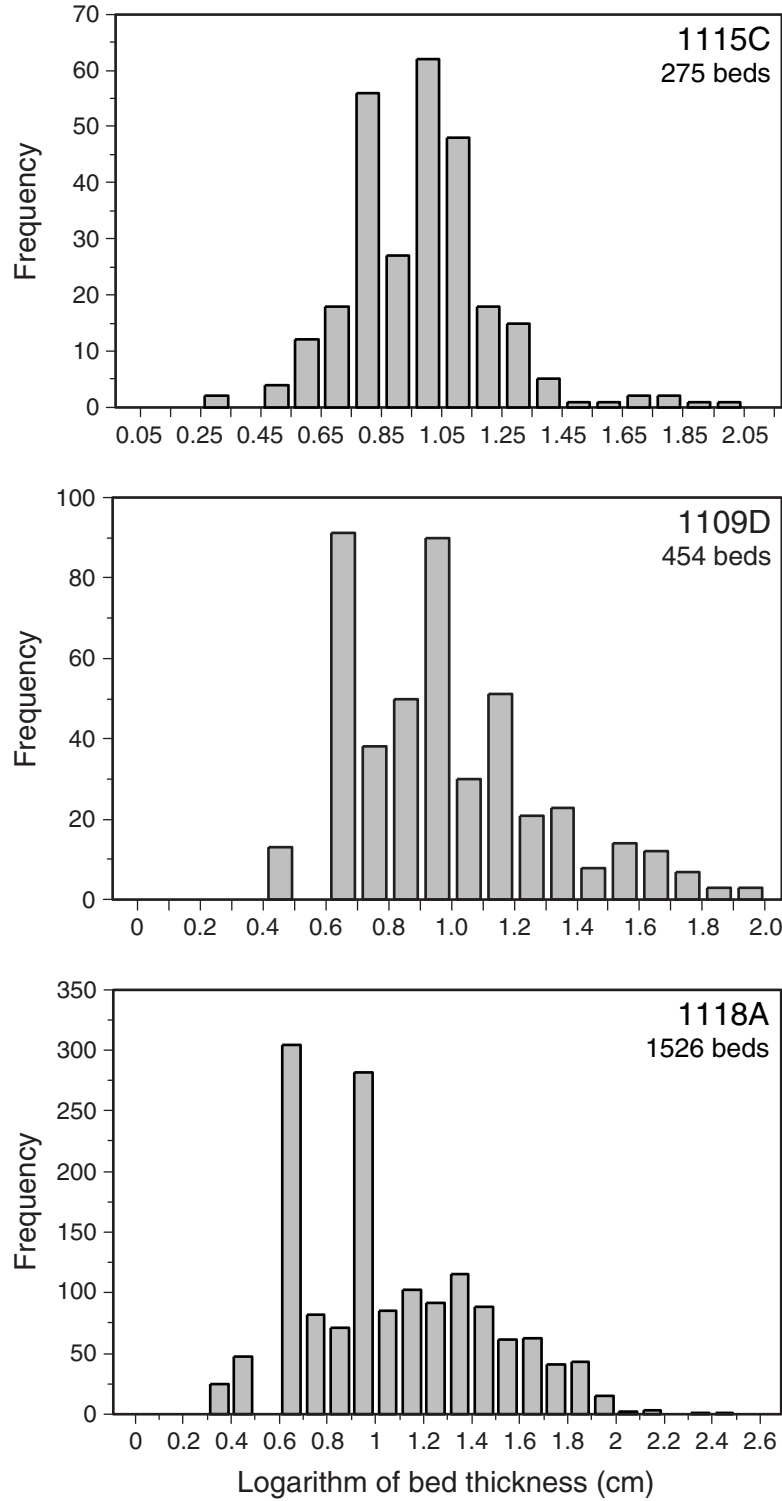


Figure F11. Plots showing exponential decline of bed thicknesses to the right of a mode in the thinnest beds. Class width = 5 cm. Both sand and silt turbidites are included.

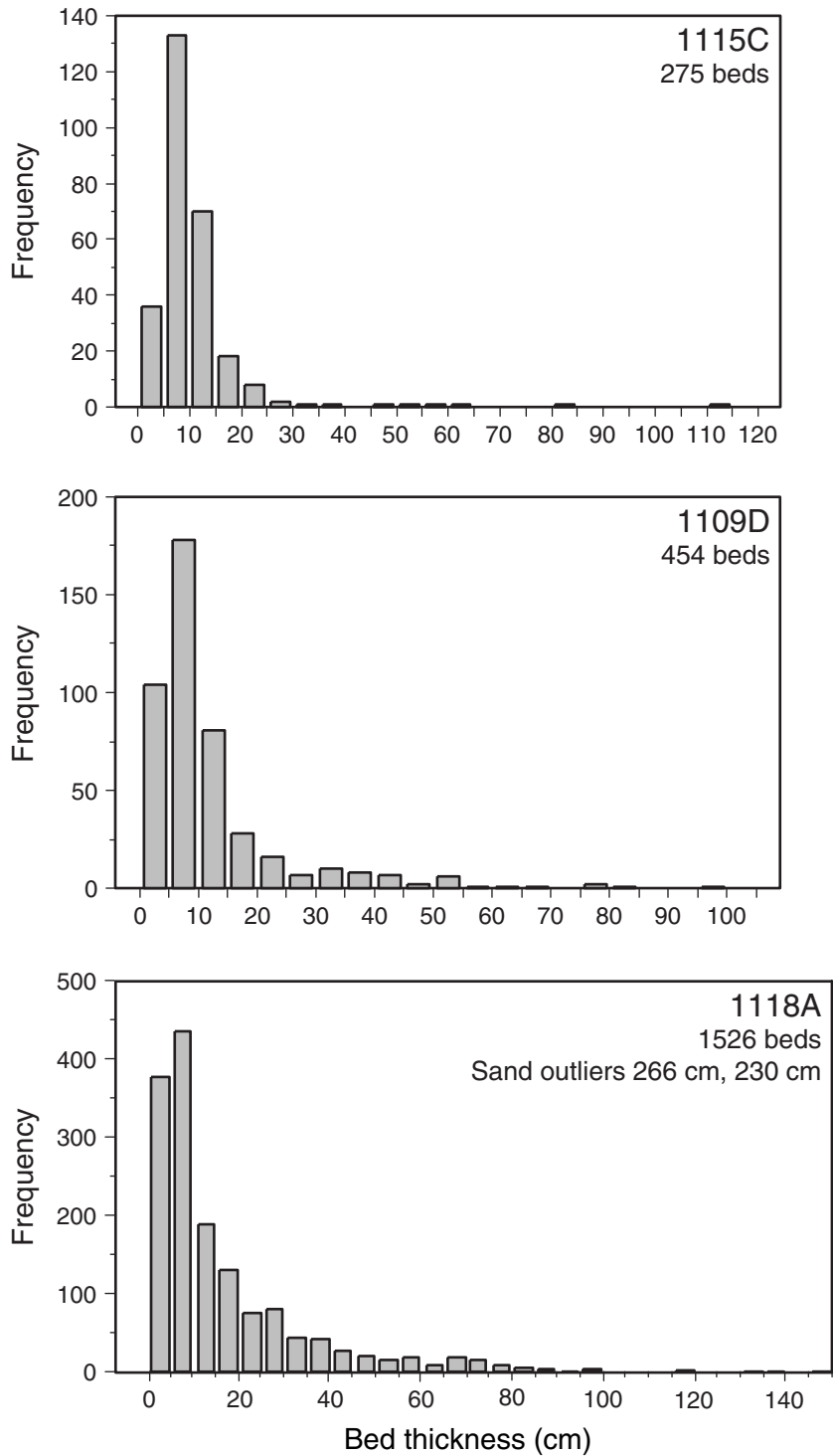


Figure F12. Logarithmic plots of the number of sand and silt beds thicker than T , vs. T , for data derived from FMS images. As predicted for power-law distributions, the data plot as straight-line segments with a slope that is the characteristic exponent of the distribution (Equation 2). A. Hole 1118A. B. Hole 1109D. C. Hole 1115C.

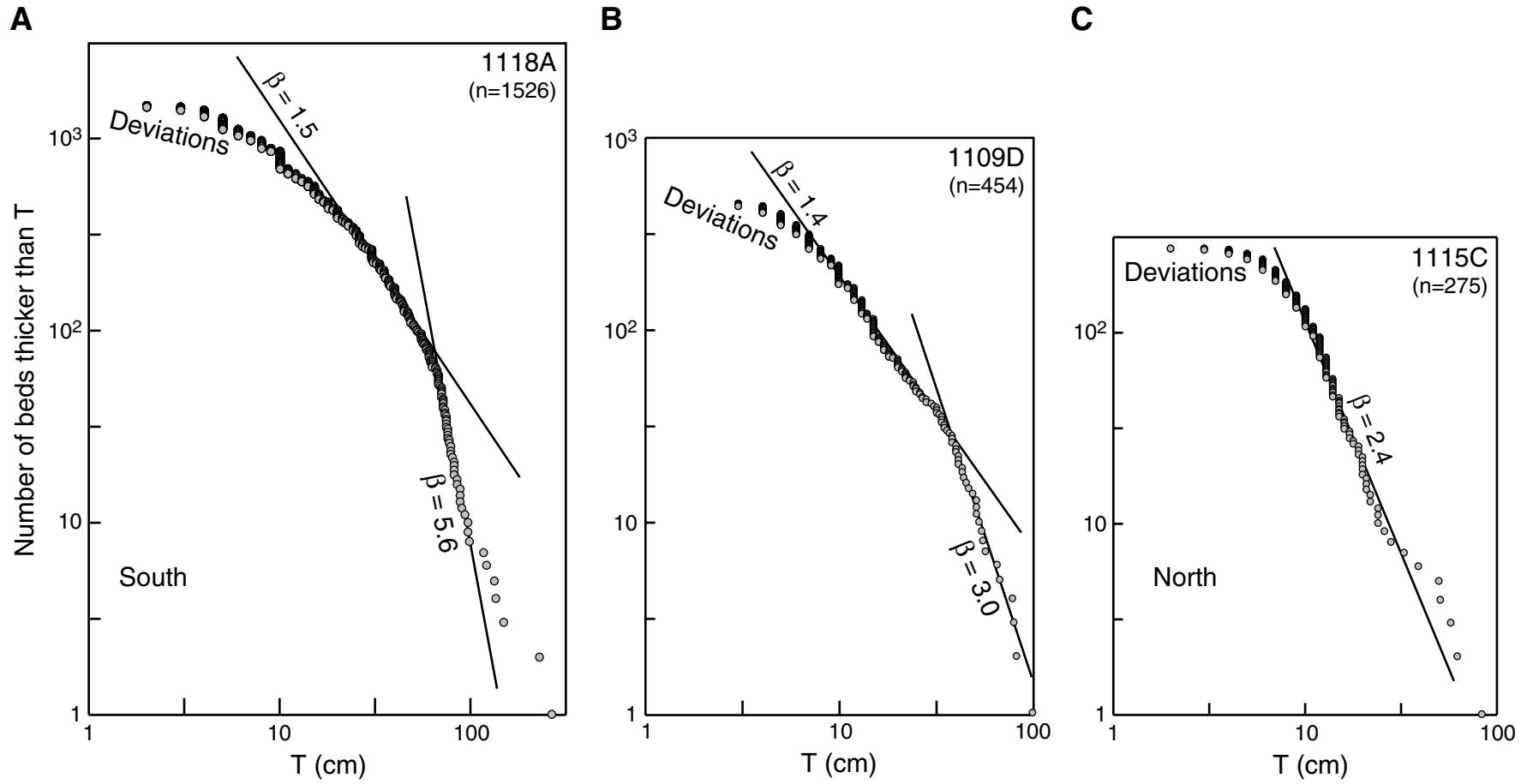


Figure F13. Plots of turbidite bed number (above the base of each column in Fig. F4, p. 16) against the age of the base of each bed, using age picks from Table T1, p. 29 (extracted from Takahashi et al., this volume). Between age picks (circles along curves), accumulation rates are assumed to be constant. Each plot shows the rate at which turbidite beds were added to the stratigraphic succession. Across the “gaps” in Hole 1109D (no FMS data or very poor quality images), the slope of the growth curve is constrained by adjacent segments of the curve. See “Turbidity-Current Frequencies,” p. 6, in “Results” for discussion.

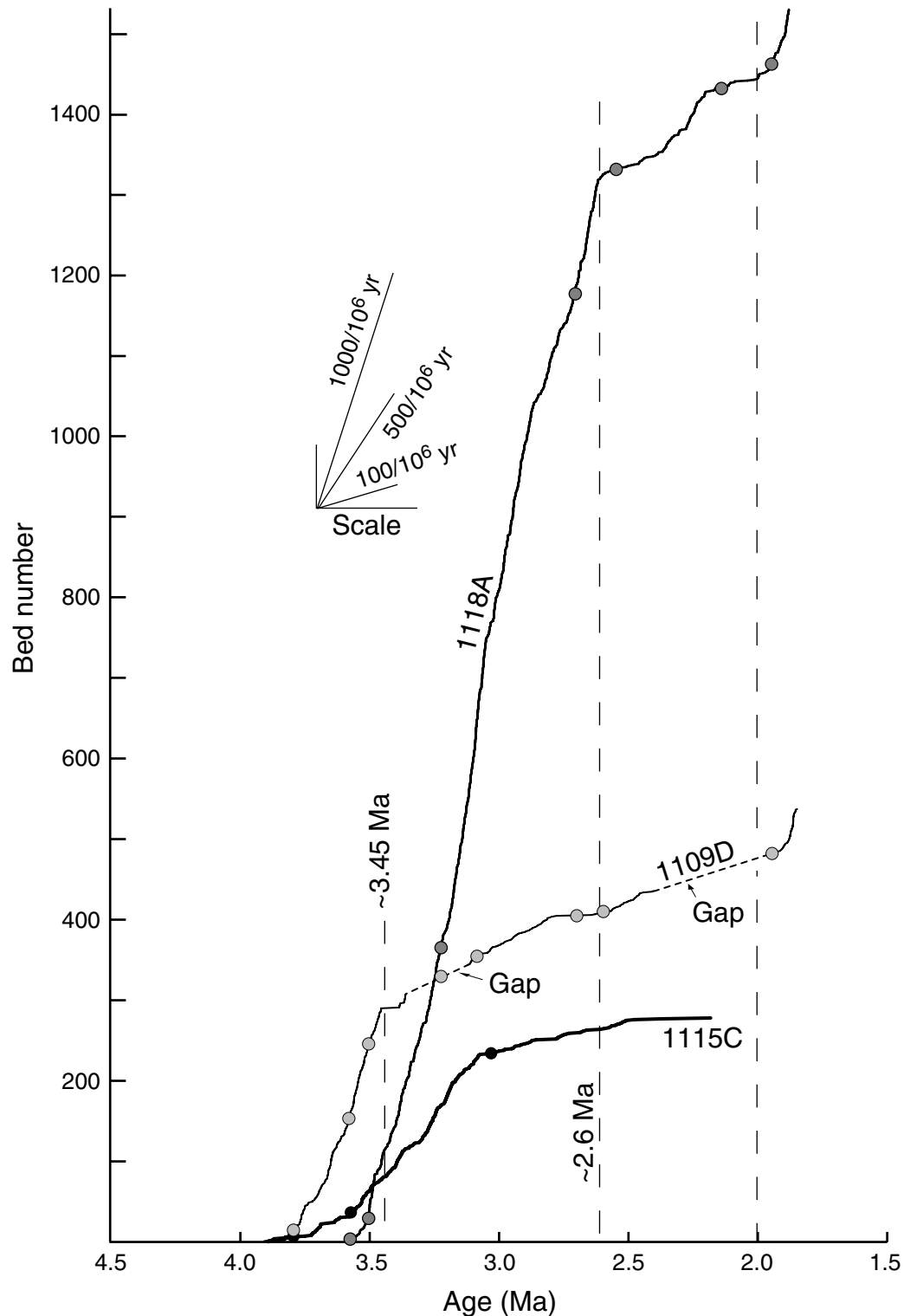


Figure F14. Multichannel seismic profile between Sites 1118 and 1109, with selected depths below the seafloor from Taylor, Huchon, Klaus, et al. (1999, their figure F25). The interval marked with a bold vertical bar is approximately three times thicker at Site 1118 than at Site 1109, confirming the preferential deposition of sandy turbidites along the axis of the rift. CMP = common midpoint.

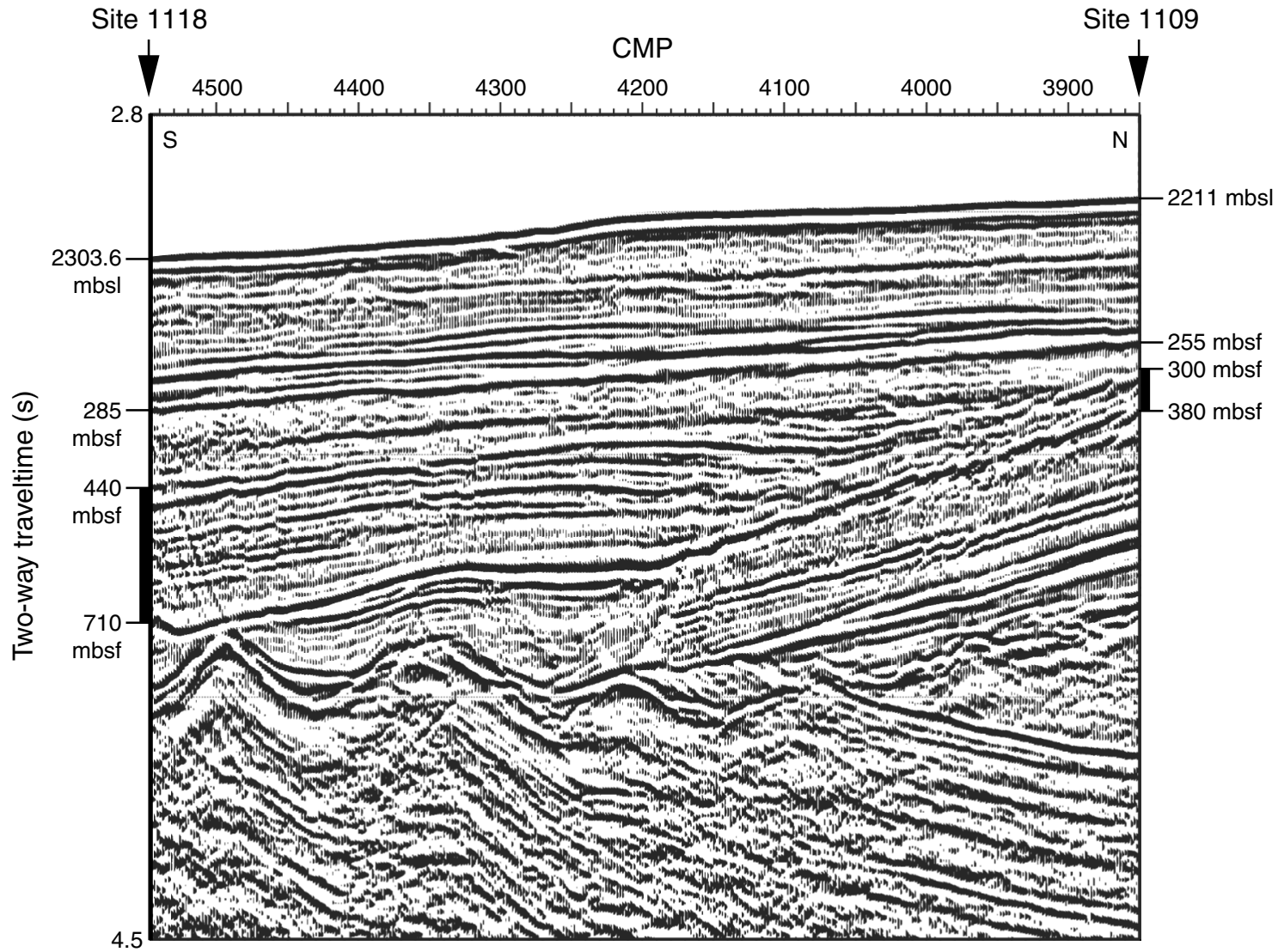


Table T1. Age picks used to constrain accumulation rates of turbidites.

| Depth (mbsf) | Age (Ma) | Turbidite bed number |
|--------------|----------|----------------------|
| 180-1109D- | | |
| 213.00 | 1.77 | NA |
| 255.00 | 1.95 | 402 |
| 291.00 | 2.58 | 376 |
| 296.50 | 2.70 | 370 |
| 331.70 | 3.09 | 320 |
| 357.00 | 3.22 | 309 |
| 443.25 | 3.50 | 248 |
| 469.61 | 3.58 | 152 |
| 550.14 | 3.80 | 9 |
| 562.61 | 3.94 | NA |
| 180-1115C- | | |
| 103.00 | 1.95 | NA |
| 192.50 | 3.04 | 248 |
| 386.01 | 3.58 | 46 |
| 408.17 | 3.80 | 21 |
| 515.30 | 5.54 | NA |
| 180-1118A- | | |
| 210.42 | 1.77 | NA |
| 288.24 | 1.95 | 1449 |
| 334.52 | 2.15 | 1428 |
| 379.68 | 2.55 | 1329 |
| 453.62 | 2.70 | 1169 |
| 662.36 | 3.22 | 361 |
| 837.69 | 3.50 | 27 |
| 849.30 | 3.58 | 2 |

Note: NA = beyond range of bed-by-bed section, but used to constrain accumulation rate at start or end of the section.

CHAPTER NOTE*

- N1. 19 February 2002—Robertson, A.H.F., Awadallah, S., Gerbaudo, S., Lackschewitz, K.S., Monteleone, B., Sharp, T.R., and other members of the Shipboard Scientific Party, 2001. Evolution of the Miocene–Recent Woodlark rift basin, SW Pacific, inferred from sediments drilled during Ocean Drilling Program Leg 180. *In* Wilson, R.C.L., Whitmarsh, R.B., Taylor, B., and Froitzheim, N. (Eds.), *Non-Volcanic Rifting of Continental Margins: A Comparison of Evidence from Land and Sea*, Spec. Publ.—Geol. Soc. London, 187:335–372.